Dysregulated CD200-CD200R signaling in early diabetes modulates microglia-mediated retinopathy

Charles W. Pfeifer[a,b] (ID), James T. Walsh[a,c] (ID), Andrea Santeford[a] (ID), Joseph B. Lin[a,b] (ID), Wandy L. Beatty[d], Ryo Terao[a,e] (ID), Yizhou A. Liu[a] (ID), Keitaro Hase[a] (ID), Philip A. Ruzycki[a,f] (ID), and Rajendra S. Apte[a,g,h,1] (ID)

Diabetic retinopathy (DR) is a neurovascular complication of diabetes. Recent investigations have suggested that early degeneration of the neuroretina may occur prior to the appearance of microvascular changes; however, the mechanisms underlying this neurodegeneration have been elusive. Microglia are the predominant resident immune cell in the retina and adopt dynamic roles in disease. Here, we show that ablation of retinal microglia ameliorates visual dysfunction and neurodegeneration in a type I diabetes mouse model. We also provide evidence of enhanced microglial contact and engulfment of amacrine cells, ultrastructural modifications, and transcriptome changes that drive inflammation and phagocytosis. We show that CD200-CD200R signaling between amacrine cells and microglia is dysregulated during early DR and that targeting CD200R can attenuate high glucose-induced inflammation and phagocytosis in cultured microglia. Last, we demonstrate that targeting CD200R in vivo can prevent visual dysfunction, microglia activation, and retinal inflammation in the diabetic mouse. These studies provide a molecular framework for the pivotal role that microglia play in early DR pathogenesis and identify a potential immunotherapeutic target for treating DR in patients.

diabetes | retinopathy | microglia | inflammation | retina

Diabetic retinopathy (DR) is a leading cause of blindness in adults (1, 2). Diagnosis and treatment of DR primarily focus on microvascular changes as they can be identified through clinical examination and targeted with current therapeutics (3). However, laboratory and clinical evidence demonstrate that retinal inflammation and neuronal alterations may precede vasculopathy and contribute to neurodegeneration and vision loss during early stages of DR (4–7). While changes in vascular permeability have been reported during early stages of DR, neuronal changes in early disease are difficult to visualize through fundoscopic examination (8). Furthermore, currently approved therapeutic strategies for treating advanced DR primarily target vascular complications, require frequent pharmacologic or ablative laser treatment, and do not reverse retinopathy in the long term (9–12). Given the immense impact of DR on global health and the inability of current treatment strategies to restore neuroretinal structure and function, there remains a significant knowledge gap in our understanding of the cellular mechanisms underlying early DR pathogenesis.

Microglia are central nervous system (CNS) tissue–resident macrophages that regulate synaptic homeostasis, cellular debris and waste removal, and immune surveillance in the retinal parenchyma (13–15). In homeostasis and disease, microglia receive patterns of molecular cues within the tissue milieu and respond through dynamic activation and function (16–20). In the retina, these heterogeneous phenotypes have been shown to directly impact neuronal function and survival, supporting further investigation of these sentinel cells in the context of retinal disease (21–23). Morphological characteristics of microglia activation have been observed in the retinas of diabetic patients and animal models during early stages of DR, and are thought to indicate a response to hyperglycemia and inflammation in the diabetic retina (24–27). In an animal model of these conditions, microglia contribute to acute loss of retinal ganglion cells (RGC) and vascular degeneration but precise characterization of the innate microglia response to hyperglycemia and the molecular mechanisms that drive this phenotype have yet to be elucidated (28). Here, we examine the role of microglia as key regulators of visual dysfunction and retinal neurodegeneration in a hyperglycemia-driven model of DR.

While the role of inflammation in DR has been extensively studied, the specific contribution of resident microglia to early disease progression has yet to be examined. During vascular stages seen later in the life cycle of DR, the blood–retina barrier (BRB) is compromised and diverse classes of non-resident immune cells infiltrate, making it difficult to distinguish the relative contributions of the resident and systemic immune cell populations to disease

Significance

We describe the detrimental contributions of retinal microglia to retinopathy in early diabetes in the mouse, identify a dysregulated neuron-microglia signaling axis that underlies these contributions and is amenable to pharmacotherapeutic intervention, and create a framework for future studies of microglia in diabetic retinopathy and other central nervous system diseases.

progression (29, 30). Furthermore, macroglial cell types such as Müller glia and astrocytes are implicated in DR but how their involvement emerges temporally, and whether they collaterally influence microglia, has yet to be resolved (31–33). Therefore, early-stage DR may provide the opportunity to interrogate the innate response of resident microglia prior to the emergence of later-stage disease elements. Furthermore, the plasticity of microglia makes them an attractive therapeutic target for early-DR intervention strategies that may preserve retinal neurons and vision as well as prevent later-stage pathology (34–36). To this end, molecular mechanisms underlying microglia-mediated features of DR present immense value in assessing immunotherapeutic strategies for treating patients.

In this study, using a streptozotocin-induced (STZ) diabetes mouse model, we demonstrate that microglia are potent drivers of retinal dysfunction and neurodegeneration during early stages of DR. We also provide evidence of increased contact with and engulfment of amacrine cells and synapses by DR-associated microglia as a contributing facet of retinopathy. In evaluating transcriptomic changes in retinal microglia, we identify patterns consistent with pro-inflammatory signaling and phagocytosis. Furthermore, we identify dysregulation of amacrine cell CD200 and microglial CD200R with associated neuroinflammation in DR. We demonstrate that CD200Fc, a CD200R agonist, can suppress high glucose-induced inflammation, transcriptomic changes, and phagocytosis in cultured microglia. Last, we show that CD200Fc also ameliorates visual dysfunction, microglial activation, and retinal inflammation during early-stage DR in the STZ mouse. Importantly, we present these findings in the absence of observable changes to vascular structure, macroglial reactivity, or immune composition in the retina. These studies provide unique molecular insight into how pathologically activated microglia are primary contributors to hyperglycemia-induced retinopathy prior to later-stage pathology and a therapeutic strategy for treating early-stage DR in the mouse and potentially in patients.

Results

Microglia Activation Occurs with Intact Blood–Retina Barrier and Normal Immune Cell Composition during Early Diabetic Retinopathy. Altered morphologies and laminar localization of microglia have been previously observed during early stages of DR in the retinas of diabetic patients and animal models, but the features of DR that trigger this phenotype are unclear. STZ-induced early-stage DR has been shown to promote retinal transcriptome changes reflective of neurovascular degeneration and inflammation (37). Thus, we first assessed whether or not compromised structural elements of the BRB and infiltrating immune cells may indirectly promote morphological activation of resident microglia. To test this, we longitudinally evaluated retinal immune cell composition and BRB components in STZ-treated $Cx3cr1^{GFP/+}$ mice during the canonical early stage of DR in the STZ model (onset—8 wk) (Fig. 1A). In line with previous studies using this model, STZ-injected animals displayed hyperglycemic blood glucose levels within 1 wk of treatment and static weight trends compared to normoglycemic vehicle-injected animals that persisted for the duration of the study (SI Appendix, Fig. S1A) (38). To characterize the immune cell profile of the retina, we applied a comprehensive antibody panel to retinal single-cell suspensions generated from diabetic (4-wk STZ, 8-wk STZ) and control animals using flow cytometry (SI Appendix, Fig. S1B). Overall immune cell counts (CD45$^+$) were not altered during the course of hyperglycemia (Fig. 1B). Control retina suspensions revealed that microglia (CD45^{lo}, CD11b$^+$, CX3CR1$^+$) made up the vast majority (>90%) of the immune cell fraction, with minor fractions of natural killer

(NK; CD45^{hi}, NK1.1$^+$) cells, neutrophils (NΦ; CD45^{hi}, Ly6G$^+$), T cells (CD45^{hi}, TCRβ$^+$), B cells (CD45^{hi}, B220$^+$), dendritic cells (DC; CD45$^+$, CD11c$^+$, CD11b$^-$), CD11c$^+$ macrophages (CD11c$^+$ Mφ; CD45$^+$, CX3CR1$^+$, CD11b$^+$, CD11c$^+$), and border-associated macrophages (BAM; CD45$^+$, CD11b$^+$, CX3CR1$^+$, MHCII$^+$). Analysis of these immune cell fractions showed no significant changes in immune cell-specific proportions during early DR.

Next, we performed fundus imaging and immunostaining to examine potential changes to other components of the BRB during early DR. Fluorescein angiography and lectin staining did not demonstrate vascular leakage or alterations in vessel structure among control or diabetic groups (Fig. 1 C and D). In surveying macroglial subtypes, astrocyte density and coverage of primary arteriole vessels, as well as Müller glia density and reactivity, were also unchanged across all tested mouse groups (Fig. 1E). However, upon assessing temporal changes in microglia morphology, we found that microglia in the plexiform niches displayed significantly reduced cell area and volume, combined process length, and branching as early as 4 wk after onset of STZ-induced hyperglycemia compared to controls (Fig. 1 F and G and SI Appendix, Fig. S1 D and E). Since flow cytometry analysis revealed no change in retinal microglia counts during early-stage DR, we hypothesized that the apparent loss in microglia density in the plexiform layers could be explained by changes in spatio-temporal distribution within the retinal laminae (SI Appendix, Fig. S1C). Indeed, retinal cross-sections revealed that microglia soma density was significantly reduced in the outer plexiform layer (OPL) and increased in the inner nuclear (INL) and ganglion cell layers (GCL) of the inner retina during early stages of DR compared to controls (Fig. 1 H and I). Microglia somas contained within inner retina neuronal layers exhibited a cross-laminar orientation compared to the typical uniplanar morphology, suggesting migratory behavior.

Despite reports of their perturbation during established stages, our findings suggest that vascular elements, macroglia, and local immune composition remain unchanged during the early stage of STZ-induced DR. However, robust alterations to microglia size, ramification, and spatio-temporal distribution occur during this period, with regional recruitment of microglia to inner retinal neuronal layers that undergo neurodegeneration in early DR. These data suggest that aberrant microglial localization might be involved in functional retina changes during early stages of DR and support the use of $Cx3cr1$-based strategies to further evaluate these cells.

Chronic Microglia Ablation Prevents Visual Dysfunction and Neurodegeneration. One of the earliest features of DR in patients and animal models is progressive degeneration of inner retinal neurons and visual function deficits as measured by retinal electrophysiological output (4, 39, 40). In observing enhanced migration of microglia into the inner retina, we proposed that microglia might play a role in early loss of inner retinal structure and function. To test this, we used $Cx3cr1^{CreER-YFP/+}$; $Rosa26^{DTA/+}$ mice to induce sustained microglia ablation in the retina through continuous administration of tamoxifen-infused chow (SI Appendix, Fig. S2A). We combined STZ and vehicle injections with regular or tamoxifen-infused chow to compare diabetic animals that were retinal microglia-depleted or retinal microglia–privileged, while controlling for potential phenotypes related to Cre activity and microglia ablation in healthy retinas (Fig. 2A). In diabetic and non-diabetic animals, tamoxifen-induced ablation of microglia did not induce changes to weight or blood glucose that differed from regular chow–fed mice through 8 wk (SI Appendix, Fig. S2B). In assessing microglia ablation efficacy, we found that tamoxifen-treated
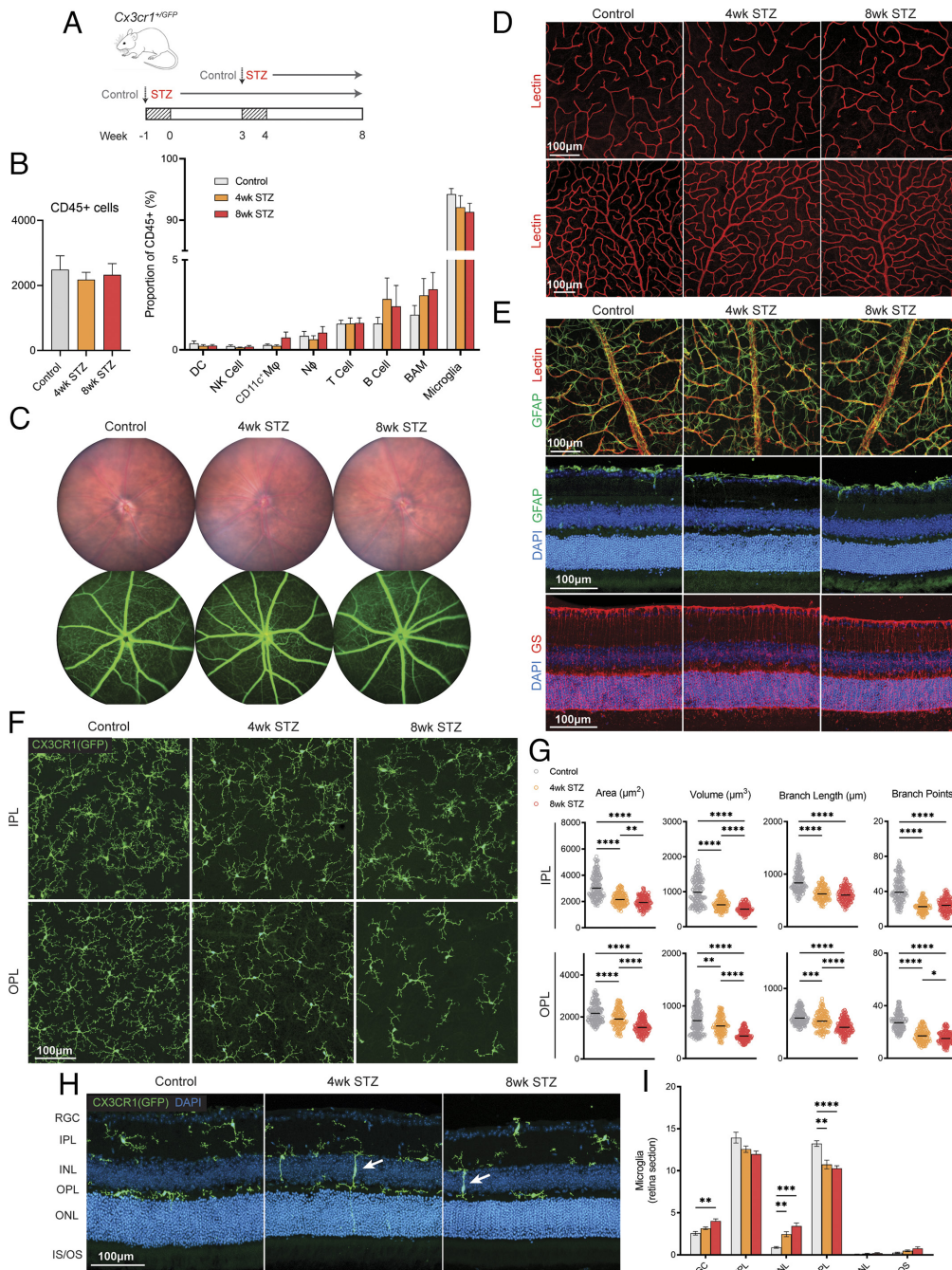
Fig. 1. Microglia activation occurs with intact blood–retina barrier and normal immune cell composition during early diabetic retinopathy. (*A*) Schematic of injection schedule for *Cx3cr1*[+/GFP] mouse groups. (*B*) Bar graphs showing raw CD45+ cell counts (*Left*) and CD45+ immune cell fractions (*Right*) for mouse retinal single cell suspensions. Each bar (n = 7 mice per group) indicates the mean ± SEM cell count or proportion of CD45+ cells. Statistical significance among groups for each cell type was determined using the Kruskal–Wallis test. (*C*) Representative images of mouse eyes using the Phoenix Micron IV retinal imaging microscope equipped with bright field (*Top*) and angiography (*Bottom*) modalities taken before (*Top*) and after (*Bottom*) sodium fluorescein injection. (*D*) Representative confocal images of intermediate (*Top*) and deep capillary plexus (*Bottom*) vascular lamina. (*E*) Representative confocal images of astrocyte density and end-feet coverage of primary arteriole vessels (*Top*), GFAP reactivity (*Middle*), and Müller glia density (*Bottom*). (*F*) Representative confocal images showing microglia morphology and organization in the IPL and OPL of mouse retinas. (*G*) Dot plots showing filament area, volume, cumulative branch length, and branch points of reconstructed microglia in control and STZ retinas. Each plot (OPL, n = 146 to 201 cells per group; IPL, n = 141 to 181 cells per group) indicates the median with each dot representing one microglia cell. Statistical significance among groups for the IPL and OPL was determined using the Kruskal–Wallis test followed by Dunn's post hoc test for multiple comparisons. (*H*) Representative confocal images and bar graph (*I*) showing microglia soma counts in individual layers of control and STZ retinas. White arrows point to microglia in trans-laminal orientation. Each bar (n = 8 to 10 mice per group) indicates the mean ± SEM of microglia soma counts per retina section. Statistical significance among groups for each retina layer was determined using Brown–Forsythe and Welch's ANOVA tests followed by Dunnett's T3 post hoc test for multiple comparisons (*$*P < 0.05$; $**P < 0.01$; $***P < 0.001$; $****P < 0.0001$*).

mice exhibited >93% reduction in retinal microglia density through 8 wk of treatment (Fig. 2 *B* and *C*). Importantly, this model of ablation allowed us to maintain a microglia-ablated retina without the confounding effects of residual microglia repopulation or neuroinflammatory phenotypes associated with other models of microglia ablation (41–43).

We next examined visual function and retinal thickness in mouse groups following early-stage DR. Anesthetized animals from all four cohorts were administered a scotopic (dark-adapted) and photopic (light-adapted) electroretinogram (ERG) to assess various components of rod- and cone- photoreceptor driven visual responses (*SI Appendix*, Fig. S2C). As expected from previous reports, photopic b-wave amplitudes were not significantly different among all groups, but scotopic a- and b-wave amplitudes were significantly reduced in STZ mice compared to each of the two normoglycemic groups (control and DTA) (Fig. 2D). In normoglycemic mice, tamoxifen treatment had no effect on measured

ERG parameters; however, scotopic a- and b-wave amplitudes surprisingly showed a partial rescue in STZ DTA mice compared to STZ mice. Similarly, the response latency of individual oscillatory wave potentials (OP) filtered from ERG waveforms (OP1-4) was increased in STZ mice compared to control mice as reported previously but were completely rescued in STZ DTA mice (Fig. 2*E*) (44). We next examined histology sections of retinas from these mice and found that, in agreement with other studies, the retinas of STZ mice were significantly thinner compared to those of controls, particularly the inner retina (Fig. 2 *F* and *G*). However, STZ DTA mouse retina thickness was significantly increased compared to STZ mice, indicating microglia ablation rescues early DR-associated neurodegeneration of the inner retina. Last, we performed standard fundus imaging and fluorescein angiography of mice but did not find any evidence of retinal lesions or vascular leakage in any groups (*SI Appendix*, Fig. S2D). Taken together, these data demonstrate that chronic
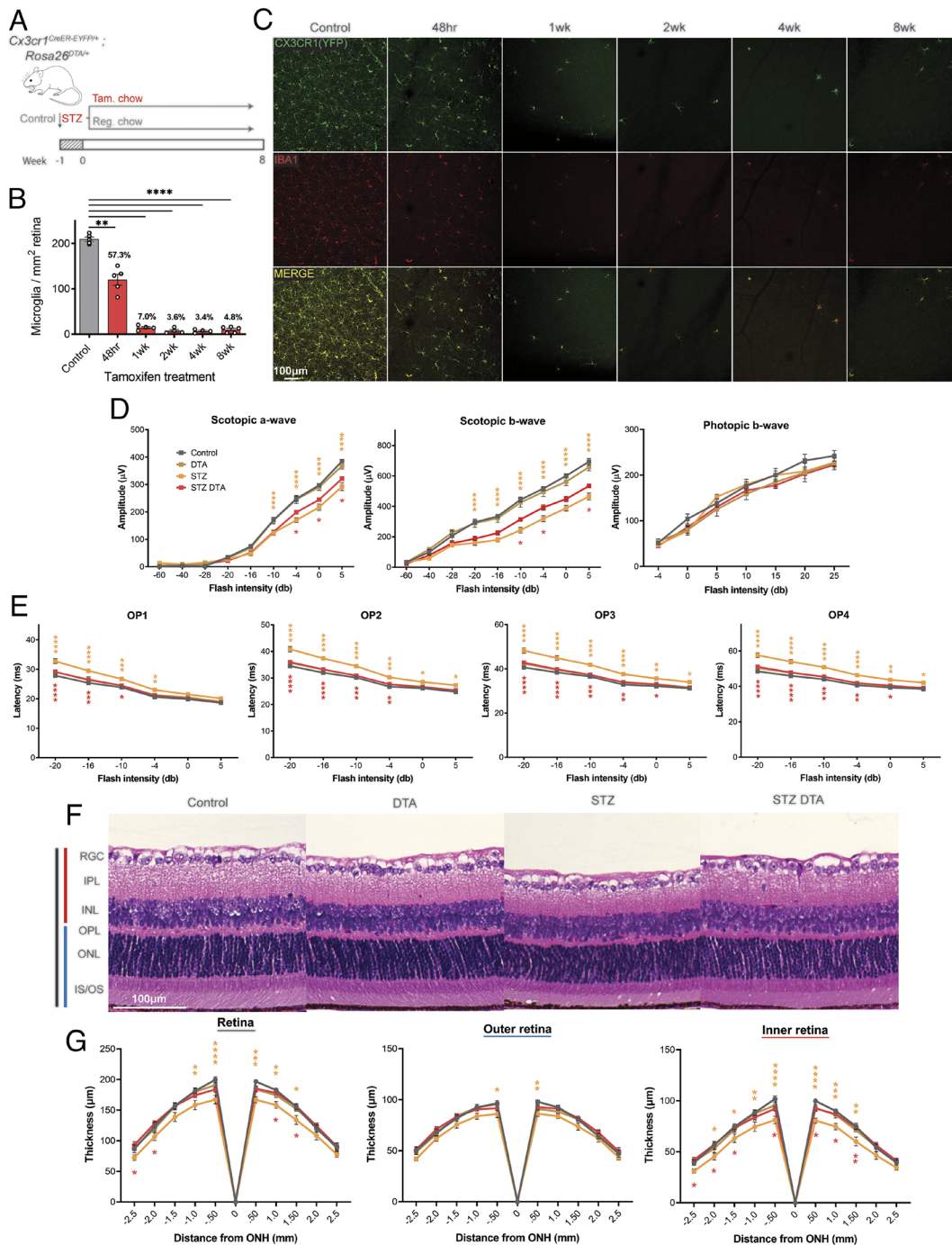
Fig. 2. Chronic microglia ablation prevents visual dysfunction and neurodegeneration. (*A*) Schematic of injection and feeding schedule for *Cx3cr1*^CreER-YFP/+^; *Rosa26*^DTA/+^ mice. (*B*) Bar graph and (*C*) representative confocal images showing retinal microglia (CX3CR1⁺, IBA1⁺) density in the retinas of control and tamoxifen-treated *Cx3cr1*^CreER-YFP/+^;*Rosa26*^DTA/+^ mice. Each bar (n = 4 to 5 mice per group) indicates the mean ± SEM of microglia counts per standardized area of the retina. Statistical significance among groups was determined using Brown–Forsythe and Welch's ANOVA tests followed by Dunnett's T3 post hoc test for multiple comparisons. (*D*) Line graphs showing scotopic a- and b-wave, and photopic b-wave amplitudes for tested light intensities. (*E*) Line graphs showing scotopic OP latencies for tested light intensities that elicit Ops (−20 to 5db). Each line (n = 8 mice per group) indicates the mean ± SEM amplitude (*D*) or latency (*E*). Statistical significance among groups was determined using two-way ANOVA tests followed by Bonferroni's post hoc test for multiple comparisons. (*F*) Representative confocal images of paraffin-embedded hematoxylin and eosin-stained (H&E) retina sections and (*G*) spider plots showing retinal layer histology and thickness for tested mouse groups. Black, blue, and red vertical lines indicate entire, outer (OPL/ONL/IS/OS), and inner (RGC/IPL/INL) retina, respectively. Each line (n = 7 to 8 mice per group) indicates the mean ± SEM retina thickness at incremental distances from the ONH. Statistical significance among groups was determined using two-way ANOVA tests followed by Bonferroni's post hoc test for multiple comparisons. Orange asterisks in (*D*, *E*, and *G*) indicate multiple comparisons test results between STZ and CTRL groups while red asterisks indicate results between STZ DTA and STZ groups (*$P < 0.05$; **$P < 0.01$; ***$P < 0.001$; ****$P < 0.0001$).

microglia ablation preserves components of rod-driven visual responses and retinal thinning in diabetic mice. This suggests that DR-associated microglia are significant contributors to the emergence of these functional and structural deficits associated with early-stage DR in the STZ mouse model. Furthermore, the strongly preserved oscillatory potential response timing in STZ DTA mice suggests that microglia may differentially impact certain retinal cell types that drive unique components of scotopic vision.

Microglia Promote Amacrine Cell and Inhibitory Synapse Loss through Increased Contact and Engulfment. OP responses are broadly generated from modulatory feedback pathways between bipolar cells (BPC), amacrine cells (AC), and ganglion cells (RGC) (45). Pharmacological studies have found that GABAergic and glycinergic transmission between ACs and

BPCs, in addition to AC and RGC-generated action potentials, is necessary for maintaining normal OP latency responses (46). Since neurodegeneration of these inner retinal subtypes has been reported during early stages of disease in animal models of DR, we hypothesized that rescued OP response latencies in diabetic microglia-depleted mice may indicate a causative link between microglia and selective neurodegeneration of these cell types (39, 47, 48). To test this, we performed immunostaining of these cellular subtypes and synapses in retina sections taken from mouse cohorts. We first found that BPC axon terminal density was significantly reduced in STZ and STZ DTA retinas compared to controls (*SI Appendix*, Fig. S3*A*). Similarly, RGC soma density was significantly reduced in STZ retinas, but not in STZ DTA retinas, as compared to control and DTA retinas (*SI Appendix*, Fig. S3*B*). Previous studies have shown that ACs are among the first neurons to be affected by hyperglycemia.

In line with this, we found that the density of two subtypes of ACs (CHAT$^+$, VGLUT3$^+$) that provide GABAergic, cholinergic, and glycinergic synaptic input was significantly reduced in STZ retinas compared to that of control and DTA groups (Fig. 3 A–C). Interestingly, cell densities for these AC subtypes were significantly increased in STZ DTA retinas compared to STZ, suggesting that microglia are a necessary contributor to loss of these AC cell subtypes during DR. Further, we also observed a significant reduction in GABAergic inhibitory synaptic ribbon (VGAT) density in the IPL of STZ retinas compared to controls, while STZ DTA retina density was significantly increased compared to that of STZ retinas, suggesting greater preservation of this synaptic layer (Fig. 3D). Importantly, we did not observe any significant differences in cell or synapse density staining between control and DTA groups, ruling out tamoxifen toxicity or effects related to microglia ablation in healthy retinas. These data supported our hypothesis that microglia could be contributing to the reduction of AC-driven oscillatory potential responses by mediating the loss of at least two AC subtypes and their inhibitory synapses that are necessary for normal OP responses.

During retinal degeneration, microglia migrate to sites of neurodegeneration to engulf and degrade cell debris but, if pathologically activated, can exacerbate degeneration of the neuroretina through aberrant phagocytosis and synapse remodeling (21, 49). Thus, we hypothesized that aberrant engulfment of AC subtypes by DR-associated microglia may mediate microglia-dependent AC dysfunction and loss. To test this, we performed confocal Z-stack imaging of flat-mounted retinas immunostained for AC subtypes (CHAT$^+$, VGLUT3$^+$) in 8-wk STZ and control mice, generated 3D reconstructions of image stacks, and quantified microglia-AC contact in the inner retina. Early DR led to a significant increase in the percentage of CHAT$^+$ ACs in contact with microglia (Fig. 3 E and F). Consistent with data from retina cross-sections (Fig. 3B), whole-mount quantification recapitulated significant reductions in CHAT$^+$ ACs in STZ retinas compared to control retinas. Interestingly, we also observed that morphologically activated microglia in STZ retinas displayed increased average size of contacts with CHAT$^+$ ACs. Upon further investigation, we observed instances of CHAT$^+$ AC encircling and engulfment by microglia, perhaps explaining the increased average volume of contact between these cell types (Fig. 3G and Movies S1–S3). We also found similar results for VGLUT3$^+$ ACs (*SI Appendix*, Fig. S3 C–E and Movies S4 and S5). Taken together, these data illustrate that chronic microglia ablation preserves amacrine cell subtypes and inhibitory synapse architecture. Furthermore, DR-associated microglia increase contact with and engulfment of these AC subtypes, which may explain preservation of ACs and the OP response in STZ DTA mice.

DR-Associated Microglia Display Ultrastructural Evidence of Activation, Oxidative Stress, and Synapse Remodeling. During CNS disease, chronic stress, and aging, microglia adopt unique ultrastructural features that correlate with their pathological activation and aberrant neurosynaptic remodeling (50). We hypothesized that the morphologically activated and phagocytic microglial phenotype we uncovered in the diabetic mouse retina may demonstrate similar ultrastructural remodeling and further explain their role in AC degeneration. To explore this, we prepared horizontal and vertical sections of control and 8-wk STZ retinas for transmission electron microscopy (TEM). Interestingly, we found a subtype of microglia that exhibited darkened cytoplasm, chromatin remodeling, and irregular shape in the inner retina (IPL/INL) of STZ retinas that was rarely observed in control retinas (Fig. 4A). We also frequently observed these DR-associated microglia (*dmg*) at the junction of

the INL and IPL with electron-dense processes leading into the inner retina neuropil (Fig. 4B). In horizontal retina sections, we found that these electron-dense cells and processes were observed at a significantly higher frequency in STZ retinas compared to control retinas (Fig. 4C). Furthermore, the neuropil of the IPL in the STZ retinas appeared more disorganized than that of control retinas, potentially indicating neurosynaptic degeneration. Upon further examination of DR-associated microglial ultrastructure, we also observed irregularities in mitochondria shape and cristae compared to those of control microglia, indicating potential oxidative stress (Fig. 4D). Last, DR-associated microglia in the inner retina exhibited close apposition and encircling of synaptic dyads with compromised clefts that were not observed in control retinas. Interestingly, we observed occasions of encircled synapses of ACs, as indicated by their vesicular density and cytoplasmic detail (Fig. 4E) (51). These data provide evidence of a previously reported microglial ultrastructural phenotype in the diabetic mouse retina. Additionally, the ultrastructural evidence of oxidative stress and chromatin remodeling, in addition to synapse remodeling, further supports a pathological role of activated microglia in degeneration of ACs and other neurosynaptic elements of the inner retina during early-stage DR.

DR-Associated Microglia Transcriptome Changes Support Inflammation, Phagocytosis, and Metabolic Reprogramming. Microglia adopt transcriptional signatures that reflect their dynamic functional roles during inflammation and disease (20, 52, 53). While microglia transcriptome changes have been described in a rat model of DR, we wanted to examine the microglia transcriptome longitudinally during early DR progression in the STZ mouse to assess the emerging response of microglia to hyperglycemia that may also explain their affinity for, and increased contact of, the inner neuroretina (54). To do this, we first generated purified mRNA samples from pooled microglia using fluorescence-activated cell sorting (FACS) of viable, GFP$^+$ microglia (*SI Appendix*, Fig. S4A). Following assessment of FACS event counts, RNA quantity, and purity, we performed RNA sequencing (RNA-Seq) using samples (n ≥ 3) from each diabetic (4-wk STZ, 8-wk STZ) and control condition. To validate the specificity of our FACS protocol, we first analyzed normalized gene counts and found that microglia-specific genes (*P2ry12, Tmem119, Hexb*) were among the highest expressed genes across all samples (*SI Appendix*, Fig. S4B). We then performed a standard EdgeR-limma pipeline analysis on all samples (n = 10) and compiled differentially expressed genes (DEG; >|1.5|FC; FDR < 0.05) for each diabetic condition compared to control. The resulting 825 DEGs compiled from both conditions were then used to analyze variance across samples using multidimensional scaling, which revealed consistent clustering within conditions and separation of condition clusters (Fig. 5A). Interestingly, of the 825 DEGs identified, we found that 767 resulted from analysis of 8-wk STZ vs. control conditions, while only 108 resulted from analysis of 4-wk STZ vs. control conditions, with 50 shared in both STZ conditions (Fig. 5B). We also performed hierarchal clustering based on DEGs, which further revealed a stark contrast between 8-wk STZ microglia transcriptome compared to that of control microglia, while 4-wk STZ microglia occupied a largely intermediate state (Fig. 5C). These data indicated that microglia undergo temporal changes to their transcriptome during early-stage DR that are substantially altered after 8 wk of hyperglycemia.

Next, we analyzed gene sets and biological pathway enrichment to relate transcriptional changes of microglia to potential functions in response to chronic hyperglycemia. Among the DEGs unique to
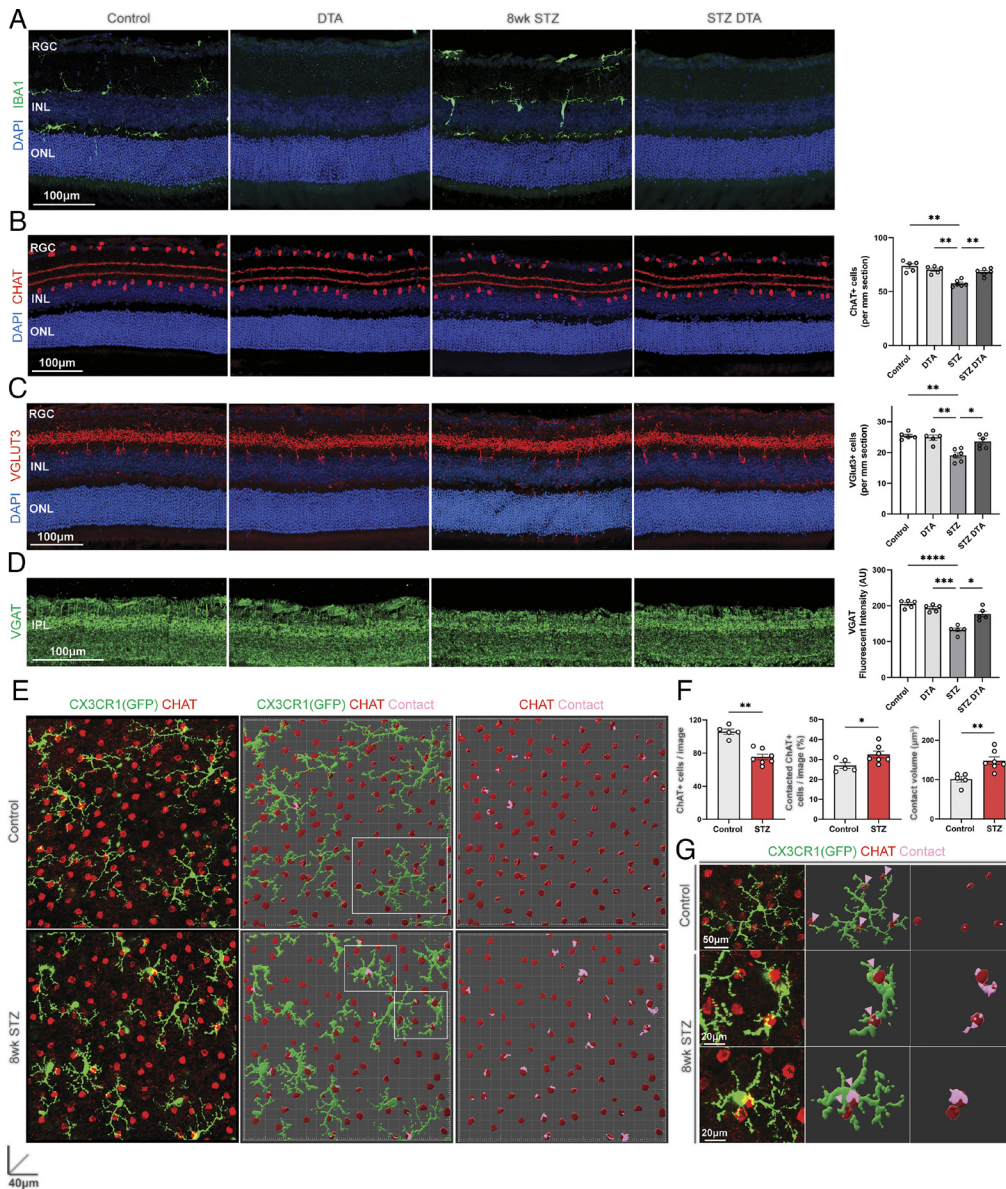
Fig. 3. Microglia promote amacrine cell and inhibitory synapse loss through increased contact and engulfment. (*A*) Representative confocal images showing (IBA1⁺) microglia in the retinas of CTRL, DTA, STZ, and STZ DTA mouse groups. (*B–D*) Representative confocal images (*Left*) and bar graphs (*Right*) showing amacrine cells (AC, CHAT⁺, VGLUT3⁺) and inhibitory synapse ribbon (VGAT⁺) density in the retinas of each mouse group. Each bar (n = 5 to 6 mice per group) indicates the mean ± SEM cell counts (*B* and *C*) or fluorescence intensity (*D*) for standardized area of the retina section. Statistical significance among groups was determined using Brown–Forsythe and Welch's ANOVA tests followed by Dunnett's T3 post hoc test for multiple comparisons. (*E*) Representative 3D reconstructions (*Middle, Right*) of confocal Z-stack images (*Left*) of flat-mounted retinas showing contacts between microglia (CX3CR1⁺) and CHAT⁺ amacrine cells in control and 8-wk STZ mouse retinas. (*F*) Bar graphs showing cell density (*Left*), contacted cells (*Middle*), and contact volume (*Right*) for CHAT+ amacrine cells in control and STZ retinas. Each bar (n = 5 to 7 mice per group) indicates the mean ± SEM. Contact volume for each mouse is an average from (n = 78 to 161) individual contacts identified in four to five confocal images of the retina. Statistical significance among groups was determined using the Mann–Whitney *U* test. (*G*) Representative images of microglia as outlined in (*E*) showing contact and engulfment profiles between microglia and CHAT-stained amacrine cells in control and STZ retinas (*P < 0.05; **P < 0.01).

the 4-wk STZ group, we identified several upregulated genes related to disease-associated microglial activation (*Cd44, Clec7a*), antigen presentation, and nuclear factor kappa B signaling pathways (*Ctse, Tnfrsf8*), and *Klf10*, an inhibitor of gluconeogenesis that increases in expression in response to high glucose levels (Fig. 5*C*) (55). In fact, several downregulated 4-wk STZ DEGs genes were those related to glucose metabolism (*Slc2a8, Idua*). In examining the DEGs unique to the 8-wk STZ group, we found that upregulated genes were primarily related to pro-inflammatory signaling and chemotaxis (*Ccl2, Ccl3, Nfkbid, Tnf, Il1b, Map3k8, Cxcl14*), as well as proliferation (*Mki67*), and lipid metabolism (*Apoc1, Ch25h*). Conversely, downregulated genes were primarily related to glycolysis (*Pkm, Pgam1, Eno1, Eno2*). Last, we analyzed genes that were differentially expressed at both time points to examine the temporal relationship between duration of hyperglycemia and changes to microglia transcriptome. While several homeostatic microglia genes were expectedly downregulated (*Fcrls, Serpine2*), we also identified commonly upregulated genes related to inflammation (*Adora1, Serping1, Cd200r4*), lipid metabolism (*Cyp4f18, B3galt1*), and insulin secretion disruption (*Igf2bp2*). To examine the larger 8-wk STZ gene set further, we ran gene ontology (GO) pathway enrichment analysis and found that biologic pathways enriched in 8-wk STZ microglia included those related to lysosome assembly, phagocytosis, and tumor necrosis factor (TNF) signaling (Fig. 5*D*). Conversely, pathways enriched in microglia derived from control samples were related to glycolysis and negative regulation of fatty acid oxidation (Fig. 5*E*). Last, we isolated a separate batch of mRNA samples to validate expression levels of genes of interest through qPCR and found that there was a disease chronicity-dependent upregulation of these genes across STZ time points (Fig. 5*F* and *SI Appendix*, Fig. S4*C*). Taken together, we show that chronic hyperglycemia induces longitudinal alterations to retinal microglia transcriptome that reflect an acute activation after 4 wk of hyperglycemia followed by a robust phenotypic shift after 8 wk. Furthermore, the phenotype described by these experiments after 8 wk favors phagocytosis, lysosomal degradation, and pro-inflammatory signaling, which is consistent with other features of DR-associated microglia described previously.

CD200R Signaling Attenuates High Glucose-Driven Microglial Inflammation and Phagocytosis In Vitro. Changes in neuroglial signaling within CNS tissue dictate microglia activation and function in disease. To identify potential signaling changes underlying pathological activation of retinal microglia and their contribution to loss of amacrine cells in STZ mice, we assessed
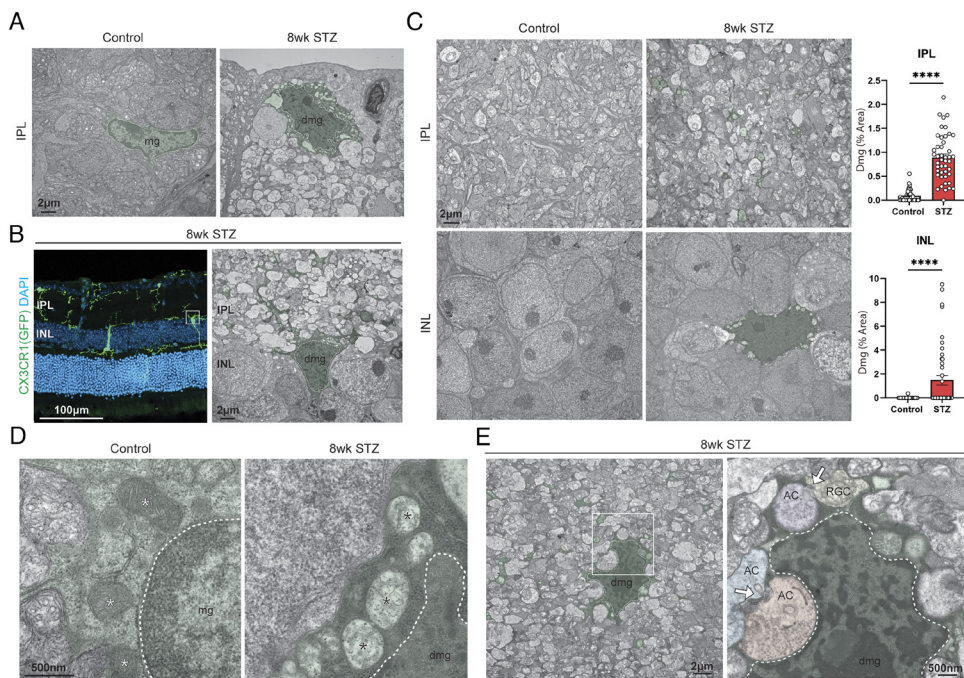
Fig. 4. DR-associated microglia display ultrastructural evidence of activation, oxidative stress, and synapse remodeling. (*A*) Representative TEM images showing IPL microglia in control *(mg)* and STZ *(dmg)* retinas shaded in green with nuclear compartments outlined with dotted white lines. (*B*) Representative confocal (*Left*) and TEM (*Right*) images of *dmg* in trans-laminal orientation positioned between the inner plexiform (IPL) and nuclear (INL) layers. (*C*) Representative TEM images (*Left*) and bar graphs (*Right*) showing *dmg* frequency in the IPL (*Left, Top* panels) and INL (*Left, Bottom* panels) of control and STZ retinas. These images are of horizontally sectioned retinas with *dmg* somas and processes shaded in green. Each bar (IPL, n = 45 images per group; INL, n = 45 images per group; n = 3 mice per group) indicates the mean ± SEM of *dmg* frequency displayed as a percentage of standardized retinal area. Statistical significance between groups was determined using the Mann–Whitney *U* test. (*D*) Representative TEM images showing microglial mitochondria labeled with white and black asterisks. (*E*) Representative low-magnification (*Left*) and high-magnification TEM image (*Right*) showing synaptic remodeling by *dmg* in the STZ retina. White arrows are directed at compromised synaptic clefts shared between amacrine cells (AC; orange, blue, purple) and ganglion cells (RGC; yellow) that are encircled by *dmg* shaded in green. (****P < 0.0001).

whether microglia transcriptome changes included dysregulation of ligand–receptor interactions. Among dysregulated 8-wk STZ DEGs from Fig. 5*B*, we identified 50 corresponding to known ligand–receptor interactions (56). We found that *Cd200r4*, which encodes the receptor CD200R4, was one of only two receptor DEGs upregulated in microglia at both diabetic time points (4-wk STZ, 8-wk STZ) (*SI Appendix,* Fig. S5 *A* and *B*). In fact, both CD200R isoforms (*Cd200r1, Cd200r4)* expressed in microglia samples showed a disease chronicity-dependent upregulation across STZ time points (*SI Appendix,* Fig. S5*C*). In models of CNS neurodegeneration and stroke, increased CD200R expression on myeloid cells, and decreased expression of cognate CD200 on neurons correlates with microglial activation, inflammation, and disease progression (57, 58). Thus, we investigated whether the CD200-CD200R axis was dysregulated in the mouse retina during early DR. Consistent with other reports, we found that in 8-wk STZ mouse retinas transcript levels of *Cd200* decreased, *Cd200r1* and *Cd200r4* increased, and inflammatory cytokines such as *Il1b* and *Tnf* increased compared to control retinas (Fig. 6*A*). Also, immunostaining for CD200R1 revealed that expression was exclusive to microglia that displayed hyperactivated morphologies in the IPL of 8-wk STZ retinas but was undetectable in control retinas (*SI Appendix,* Fig. S5*D*). We also examined endogenous sources of CD200 in the mouse retina and found that expression was detected in RGC, IPL, and INL layers. Furthermore, we found that CD200 fluorescence intensity was decreased in the retinas of 8-wk STZ mice compared to controls and similar to decreases in *Cd200* transcript (Fig. 6 *B* and *C*). In the CNS, CD200 expressed by neurons interacts with microglial CD200R to inhibit various immune responses and control microglial activation through inhibition of Ras/MAPK pathways (59). We then revisited microglia–neuron interactions in 8-wk STZ retinas and found that AC subtypes such as CHAT⁺ and AP2⁺ GABAergic ACs express CD200 in the healthy mouse retina (*SI Appendix,* Fig. S5 *E* and *F*). However, 8-wk STZ retinas showed both reduced numbers of CD200-expressing ACs and loss of CD200 expression in remaining ACs, suggesting that chronic hyperglycemia may decrease AC-derived

sources of CD200 in the mouse retina. Furthermore, ACs contacted by activated microglia in diabetic mouse retinas lacked expression of CD200, suggesting decreased CD200-CD200R interactions may elicit aberrant interaction and engulfment by microglia (Fig. 6*D*).

CD200R signaling with exogenous CD200 fusion protein (CD200Fc) has been shown to ameliorate microglia activation and features of disease progression (60, 61). To examine whether CD200R binding could resolve microglia-mediated neuroinflammation in diabetes, we first created a cell culture model of hyperglycemia by treating BV2 microglia cells in normal (1 g/L) or high (4.5 g/L) glucose media to mimic blood-glucose concentrations of STZ diabetic (450 mg/dL) and control (100 mg/dL) mice used in previous experiments. We also treated cells with or without CD200Fc to examine its impact on glucose-stimulated microglia (Fig. 6*E*). High glucose stimulation of microglia resulted in upregulation of nitrogen oxide species production (*Nos2*) and pro-inflammatory cytokines (*Il1b, Tnf*) similar to DR-associated microglia in vivo after 48 h. Interestingly, CD200Fc suppressed high glucose-induced production of these transcripts in a concentration-dependent manner (Fig. 6*F*). Next, we performed RNA Sequencing on purified mRNA samples from treated (50 ng/mL) and untreated BV2 microglia to interrogate broader transcriptional programs affected by CD200Fc. We used a standard EdgeR-limma pipeline analysis for all samples (n = 12) from each of the four conditions (NG, NG+CD200, HG, HG+CD200) to compile DEGs (>|1.5|FC; FDR < 0.05) for each paired comparison of interest. Using multidimensional scaling, we found consistent clustering of samples by condition but noticed that HG and HG+CD200 clusters were separated from NG and NG+CD200 clusters, which overlapped with one another (*SI Appendix,* Fig. S5*G*). Consistent with this analysis, we identified 2064 total DEGs when comparing conditions, but the majority of these resulted from comparing HG against NG (1329) and HG+CD200 against HG (748) (Fig. 6*G*). Next, we examined genes at the intersection of these comparisons to enhance our understanding of high glucose-induced gene expression patterns suppressed by CD200Fc treatment. We found 429 DEGs within this intersection that were predominantly increased when comparing HG against
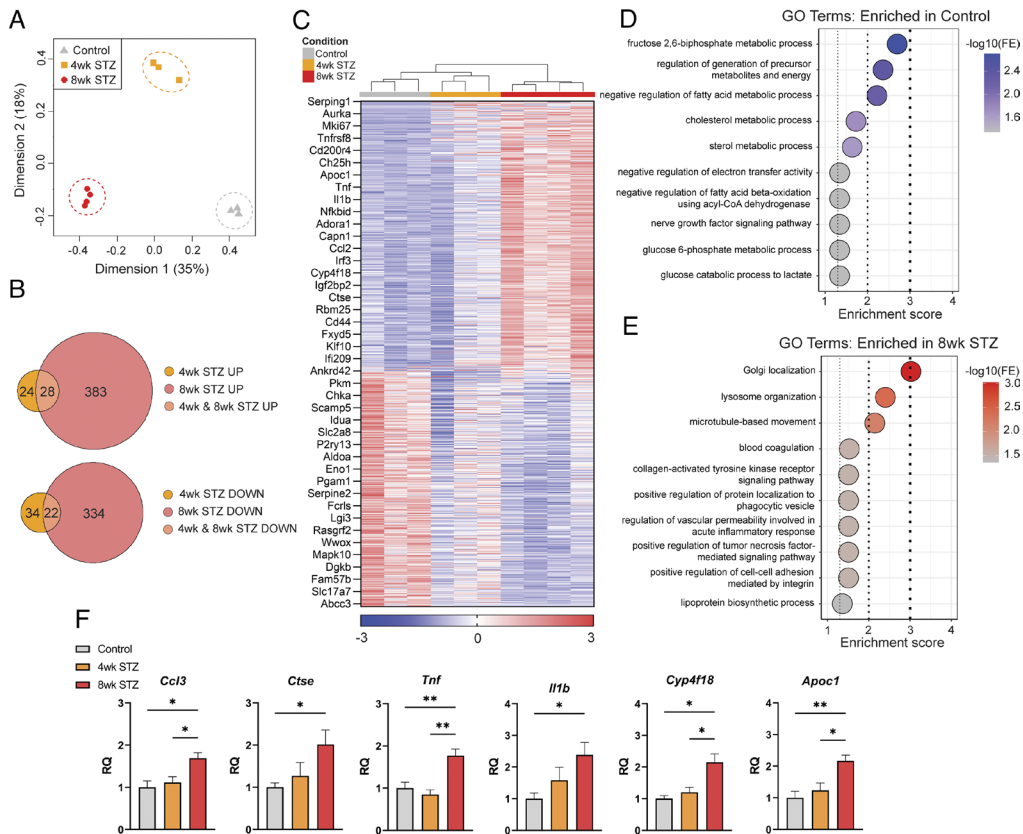
A

Control
4wk STZ
8wk STZ

Dimension 2 (18%)

Dimension 1 (35%)

B

24 | 28 | 383

4wk STZ UP
8wk STZ UP
4wk & 8wk STZ UP

34 | 22 | 334

4wk STZ DOWN
8wk STZ DOWN
4wk & 8wk STZ DOWN

C

Condition
Control
4wk STZ
8wk STZ

Serping1, Aurka, Mki67, Tnfrsf8, Cd200r4, Ch25h, Apoc1, Tnf, Il1b, Nfkbid, Adora1, Capn1, Irf3, Ccl2, Cyp4f18, Igf2bp2, Ctse, Rbm25, Cd44, Fxyd5, Klf10, Ifi209, Ankrd42, Pkm, Chka, Scamp5, Idua, Slc2a8, P2ry13, Aldoa, Eno1, Pgam1, Serpine2, Fcrls, Lgi3, Rasgrf2, Wwox, Mapk10, Dgkb, Fam57b, Slc17a7, Abcc3

-3   0   3

D

GO Terms: Enriched in Control

fructose 2,6-biphosphate metabolic process
regulation of generation of precursor metabolites and energy
negative regulation of fatty acid metabolic process
cholesterol metabolic process
sterol metabolic process
negative regulation of electron transfer activity
negative regulation of fatty acid beta-oxidation using acyl-CoA dehydrogenase
nerve growth factor signaling pathway
glucose 6-phosphate metabolic process
glucose catabolic process to lactate

-log10(FE)
2.4
2.0
1.6

Enrichment score

E

GO Terms: Enriched in 8wk STZ

Golgi localization
lysosome organization
microtubule-based movement
blood coagulation
collagen-activated tyrosine kinase receptor signaling pathway
positive regulation of protein localization to phagocytic vesicle
regulation of vascular permeability involved in acute inflammatory response
positive regulation of tumor necrosis factor-mediated signaling pathway
positive regulation of cell-cell adhesion mediated by integrin
lipoprotein biosynthetic process

-log10(FE)
3.0
2.5
2.0
1.5

Enrichment score

F

Control
4wk STZ
8wk STZ

Ccl3   *Ctse*   *Tnf*   *Il1b*   *Cyp4f18*   *Apoc1*

RQ

Fig. 5. DR-associated microglia transcriptome changes support inflammation, phagocytosis, and metabolic reprogramming. (A) Multidimensional scaling plot showing clustering of, and separation of, RNA-Seq samples (n = 3 to 4 mice per group) for control, 4-wk STZ, and 8-wk STZ conditions. (B) Euler diagrams showing the number of differentially expressed genes (DEGs) for 4-wk- and 8-wk-STZ conditions that are either increased (*Top*) or decreased (*Bottom*) in expression compared to control. (C) Heatmap showing hierarchical clustering of DEGs for all samples derived from normalized gene counts. (D and E) GO biological process pathways enriched in 8-wk STZ (D) and control (E) conditions using Fisher's exact (FE) test. (F) Bar graphs showing expression levels of genes validated by qPCR. Each bar (n = 6 to 7 mice per group) indicates the mean ± SEM of gene expression standardized to control values. Statistical significance among groups for each gene was determined using the Kruskal–Wallis test followed by Dunn's post hoc test for multiple comparisons (*$P < 0.05$; **$P < 0.01$).

NG but decreased when comparing HG+CD200 against HG (Fig. 6 *H* and *I*). Among these were genes related to inflammation (*Mmp9, Nos2, C3, Slfn4, Adgre1, Stat2, Irf7*), phagocytosis (*Marco, C3, Cd300lf*), and glycolysis (*Slc16a3, Slc2a6*). Interestingly, many of these same genes were among the most downregulated when comparing HG+CD200 against HG. We next ran Kyoto Encyclopedia of Genes and Genomes (KEGG) pathway analysis on these downregulated genes and found that the top suppressed gene sets were related to nucleotide oligomerization domain (NOD)-like receptor signaling, antigen processing and presentation, complement signaling, and phagocytosis, suggesting that CD200Fc potently inhibits high glucose-induced transcription underlying inflammation and scavenger-related functions in cultured microglia.

Acute high glucose exposure has been shown to stimulate surveillance and scavenging functions in BV2 microglia (62). Since CD200Fc suppressed transcriptional patterns related to phagocytosis and lysosome function in high glucose-treated microglia, we wanted to test whether microglia upregulated these functions in vitro similarly to aberrant phagocytosis observed in STZ mice in vivo. To do this, we stimulated BV2 microglia for 48 h as previously described (Fig. 6E) before exchanging for media containing isolated synaptosomes from the mouse retina tagged with pHRodo conjugated dye. After 2 h of synaptosome exposure, we found that microglia pretreated with high glucose showed a greater accumulation of fluorescent synaptosomes compared to normal glucose-treated microglia (Fig. 6 *J* and *K*). However, microglia pretreated with CD200Fc-supplemented high glucose media showed fluorescent profiles more similar to normal glucose-treated microglia. Furthermore, microglia pretreated with CD200Fc-supplemented normal glucose media showed synaptosome uptake that did not significantly differ from that of normal glucose media-treated microglia, suggesting that CD200Fc suppresses high glucose-stimulated synaptosome engulfment in vitro. These studies provide evidence of dysregulated CD200-CD200R neuroglial signaling in a mouse model of DR.

Furthermore, these in vitro experiments demonstrate that therapeutic targeting of the microglia-specific CD200R with CD200Fc can inhibit high glucose-stimulated inflammation and phagocytosis in cultured microglia.

CD200R Signaling Prevents Visual Dysfunction, Microglial Activation, and Retinal Inflammation In Vivo. Given the therapeutic potential of CD200Fc in models of CNS disease, and our demonstrations in vitro, we wanted to test whether CD200Fc could prevent features of microglia-mediated retinopathy in the STZ mouse. To do this, we administered single intravitreal injections of CD200Fc (2 μg/μL; 1.5 μL) or PBS into the eyes of control (CTRL+PBS) or 4-wk STZ (STZ+CD200Fc; STZ+PBS) mice since we previously identified robust transcriptional changes in DR-associated microglia between 4- and 8-wk STZ (Fig. 7*A*). We then assessed visual function, microglia morphology, and retinal inflammation 4 wk later (8-wk STZ). First, CD200Fc did not alter weight change or blood glucose trends in STZ mice (Fig. 7*B*). Next, we found that scotopic a- and b-wave amplitude responses were significantly increased in STZ+CD200Fc mice compared to STZ+PBS mice following mid- to high-intensity flash stimuli (–16 to 5 db) (Fig. 7 *C* and *D*). In examining microglial morphology, we expectedly observed irregularly distributed and less ramified microglia in the OPL of STZ+PBS retinas, but microglia in the OPL of STZ+CD200Fc retinas appeared highly ramified and more evenly distributed, similar to that of CTRL+PBS retinas (Fig. 7*F*). Furthermore, we observed less hyperactivated microglia in the IPL of STZ+CD200Fc retinas compared to STZ+PBS retinas. Last, we found that transcript levels of *Cd200r1* and inflammatory cytokines (*Tnf, Nos2, Il6*) were expectedly increased in STZ+PBS retinas compared to CTRL+PBS retinas, but expression levels were significantly decreased in STZ+CD200Fc retinas compared to STZ+PBS, and more similar to CTRL+PBS baselines (Fig. 7*E*). These experiments suggest that CD200Fc can prevent visual
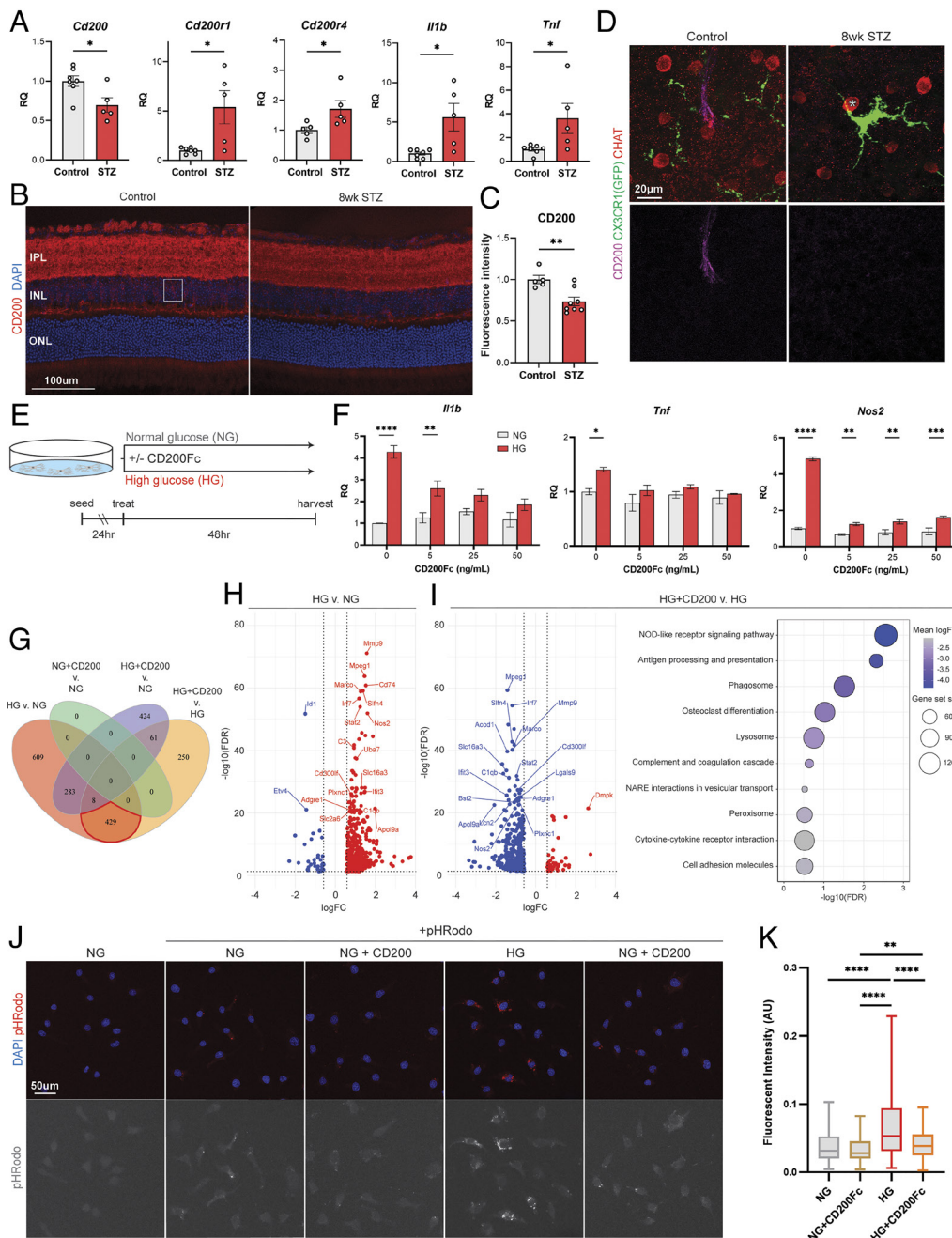
Fig. 6. CD200R signaling attenuates high glucose-driven microglial inflammation and phagocytosis in vitro. (*A*) Bar graphs showing expression levels of genes analyzed by qPCR using mouse retinal tissue. Each bar (n = 5 to 7 mice per group) indicates the mean ± SEM of gene expression standardized to control values. Statistical significance among groups for each gene was determined using the Mann–Whitney *U* test. (*B* and *C*) Representative confocal images (*B*) and bar graph (*C*) showing CD200 fluorescence intensity in the retinas of control and 8-wk STZ mice. Individual INL neuron expressing CD200 is outlined by a white square. Each bar (n = 5 to 8 mice per group) indicates the mean ± SEM fluorescence intensity standardized to control values. Statistical significance among groups for mean fluorescence was determined using the Mann–Whitney *U* test. (*D*) Representative high magnification confocal images showing CHAT+ amacrine cell CD200 expression in the INL of control and 8-wk STZ mice. CHAT+ amacrine cells contacted by activated microglia are indicated with a white asterisk. (*E*) Schematic of seeding, treatment, and harvest schedule for BV2 microglia cells. (*F*) Grouped bar graphs showing expression levels of genes analyzed by qPCR following treatment of BV2 microglia. Statistical significance among groups was determined using two-way ANOVA tests followed by Bonferroni's post hoc test for multiple comparisons. (*G*) Grouped Venn diagram showing the number of differentially expressed genes (DEGs) for each condition comparison of interest. (*H*) Volcano plot showing DEGs that are increased (red) or decreased (blue) in HG samples compared to NG samples. (*I*) Volcano plot (*Left*) showing DEGs resulting from "HG+CD200 v. HG" comparison and dot plot (*Right*) showing KEGG gene sets with the greatest average decreased expression in HG+CD200 samples compared to HG samples. (*J*) Representative images of BV2 microglia following pHRodo-tagged synaptosome treatment. (*K*) Box and whisker plot showing BV2 microglia fluorescent intensity represented in (*J*, pHRodo). Each plot (NG, n = 245; NG+CD200, n = 238; HG, n = 223; HG+CD200, n = 220) indicates the median, maximum and minimum, and interquartile range. Statistical significance among groups was determined using the Kruskal–Wallis test followed by Dunn's post hoc test for multiple comparisons (*P < 0.05; **P < 0.01; ***P < 0.001; ****P < 0.0001).

dysfunction, microglial activation, and retinal inflammation during early-stage DR in the STZ mouse. Furthermore, we show that this therapeutic effect can be achieved with a single intravitreal injection and sustained for at least 1 mo after injection.

Discussion

This study describes a cellular mechanism by which pathologically activated microglia contribute to inner retinal dysfunction and loss during early-stage DR in a mouse model of type I diabetes. Because the diabetic retina is a complex microenvironment in which to study cell type–specific contributions to disease, we implemented an early-stage model of STZ-induced DR and evaluated neuroinflammatory components in order to establish a basis for emerging retinopathy in response to chronic hyperglycemia. Through this approach, we demonstrate that morphologically

activated microglia are the first responders and concentrate in the inner retina. Utilizing chronic microglia ablation in the retina, paired with interrogation of retinal function and structure, we identify features of retinopathy that are uniquely dependent upon microglial involvement. At the intersection of these findings, we show that enhanced microglial contact and engulfment of ACs and synapses in part explain their detrimental role in early DR pathogenesis. We overlay transcriptional changes in DR-associated microglia and retina and identify the CD200-CD200R signaling axis as a potential target for suppressing microglia-mediated retinopathy. Last, using in vitro and in vivo modeling of high glucose-challenged microglia, we demonstrate that enhanced CD200R signaling via CD200Fc can dampen microglial activation, inflammation, and phagocytosis, while also preserving visual function. These experiments provide a foundation for the development of an immunotherapeutic strategy to prevent microglia-mediated
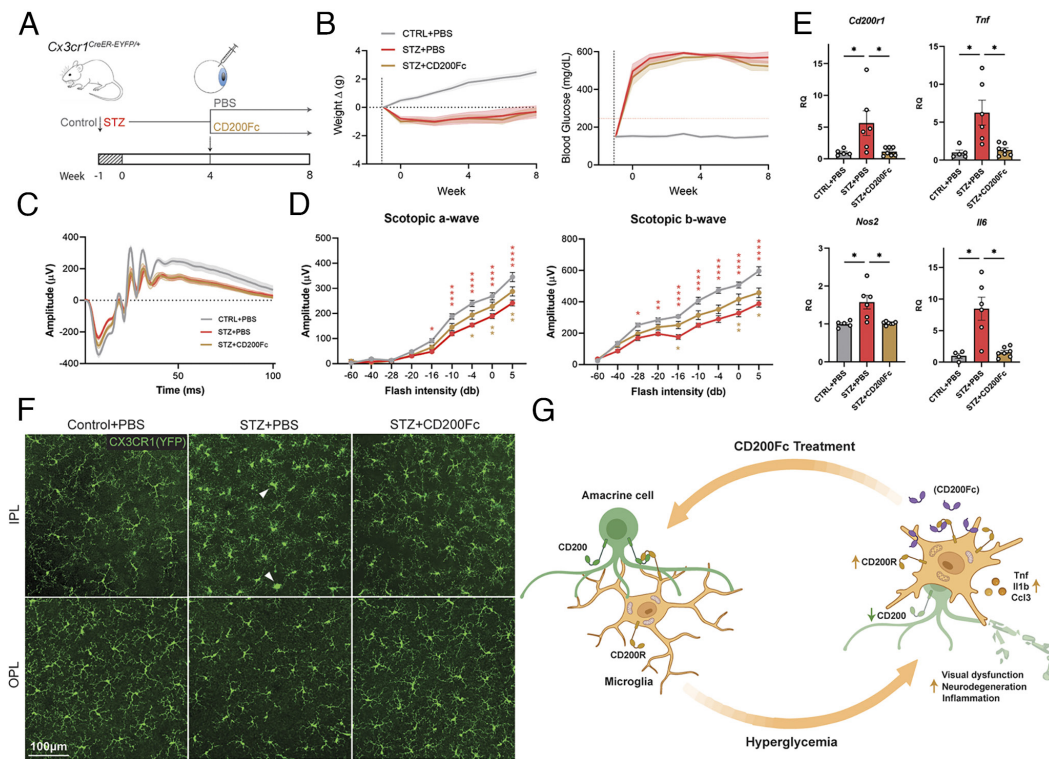
Fig. 7. CD200R signaling prevents visual dysfunction, microglial activation, and retinal inflammation in vivo. (*A*) Schematic of intraperitoneal and intravitreal injections for *Cx3cr1*^CreER-YFP/+ mice. (*B*) Line graphs showing weight change (*Left*) and blood glucose measurements (*Right*) in mouse groups. Each line (n = 7 to 9 mice per group) indicates the mean ± SEM calculated for animals used in the study. (*C* and *D*) Line graphs showing scotopic electroretinogram (ERG) response waveforms (*C*), and a- and b-wave amplitudes (*D*) for each mouse group. Data (n = 7 to 9 mice per group) indicate the mean ± SEM amplitude. Statistical significance among groups was determined using the two-way ANOVA test followed by Bonferroni's post hoc test for multiple comparisons. Red asterisks in (*D*) indicate multiple comparisons test results between STZ+PBS and CTRL+PBS groups while beige asterisks indicate results between STZ+CD200Fc and STZ+PBS groups. (*E*) Bar graphs showing expression levels of selected genes by qPCR. Each bar (n = 5 to 7 mice per group) indicates the mean ± SEM of gene expression standardized to control values. Statistical significance among groups for each gene was determined using the Kruskal–Wallis test followed by Dunn's post hoc test for multiple comparisons. (*F*) Representative confocal images showing microglia morphology and organization in the IPL and OPL of tested mouse groups. Example hyperactivated microglia are indicated by white arrowheads. (*G*) Illustration of the proposed mechanism for treating CD200-CD200R dysregulation underlying microglia-mediated retinopathy during early-stage DR via CD200Fc treatment. (*$P < 0.05$; **$P < 0.01$; ***$P < 0.001$; ****$P < 0.0001$).

neuroretinopathy in early DR and potentially other CNS diseases where microglia are implicated in neurosynaptic pathology.

We show that microglia remain the predominant immune cell type (>92%) in the retina and play a critical role in early DR pathogenesis. While it remains likely that microglia are mediating the phenotypes we observe, we cannot exclude that depletion of resident non-microglial macrophages (<1%), intravascular adherent leukocytes, and a portion of circulating monocytes via tamoxifen treatment in *Cx3cr1*^CreER-YFP/+;*Rosa26*^DTA/+ mice may also contribute to visual dysfunction and neurodegeneration (63). BRB compromise, peripheral immune cell infiltration, and macroglial activation and death are observed during established stages of DR, but we show that these facets of disease are not triggered within 8 wk of chronic hyperglycemia (4, 31, 64). However, the limited approach we use to study features such as vascular permeability does not rule out more acute vascular changes during early-stage DR that others have observed (8, 65, 66). Importantly, we present these data in the same context as the majority of previous DR rodent studies in implementing STZ to model DR (67). Multiple low-dose administration of STZ has been shown to only partially damage pancreatic islets, triggering a primarily systemic inflammatory response followed by delayed hyperglycemia. Conversely, the single high-dose STZ model used in the present study sufficiently ablates pancreatic beta cells and provides a more powerful system for examining neuroinflammation in early DR elicited by chronic hyperglycemia (68). Future work is required to examine how ablation or inhibition of other myeloid cell species impacts features of DR across various models and stages of disease.

Morphological features of microglia activation and inner retinal neurodegeneration have been previously characterized in DR, but we present evidence of these phenomena emerging in parallel and being uniquely interconnected (24, 47, 48, 69). We show that anatomically distinct populations of microglia in the plexiform layers reconfigure ramification patterns similarly, but OPL microglia

display an enhanced affinity for regions of the inner retina. Furthermore, we report that chronically ablating these cells from the diabetic retina preserves inner retinal visual function and structure. In showing that microglia increase contact and engulfment of ACs within this area of the retina, and are necessary for the lengthening of OP response latency, we suspect that these findings point to a mechanism specific to ACs. Reduced GABA activity in the brain has been shown to result in enhanced microglial activity and contact with neuronal synapses, often resulting in aberrant remodeling (70). Furthermore, inflammatory cytokines disrupt synaptic homeostasis and can trigger apoptotic cell death. To this end, we propose that dysfunctional inhibitory AC synapses during early-stage DR may in part elicit initial activation of retinal microglia. However, as we have demonstrated in other parts of this work, elicitation of a response from microglia and their subsequent contact and disposal of ACs may be dictated by different signaling mechanisms. Future work will be devoted to untangling the importance, and temporal emergence, of these potential explanations of microglia-mediated loss of ACs and synapses.

Microglial ultrastructural remodeling such as chromatin aggregation, irregular mitochondria morphology, and enhanced affinity for synaptic clefts in the inner retina may enhance our understanding of microglia function in DR. While ultrastructural phenotypes of microglia can be heterogeneous, the subtype we observe aligns with previous reports of aberrant synapse remodeling by microglia in the context of chronic stress and disease, including diabetes (50, 71, 72). Given the oxidative stress and inflammatory activation that microglia undergo in response to acute glucose fluctuations in vitro, our findings suggest that chronic hyperglycemia may induce a similarly pathologic state in vivo that results in their contribution to inner retinal neurodegeneration through aberrant synapse stripping and inflammatory cytokine production during DR (73). Future work will be focused on examining longitudinal alterations to, and

potential heterogeneity among, retinal microglia ultrastructure during DR and its impact on surrounding neuroretina.

Our RNA-Seq dataset provides further resolution of microglia activation in identifying gene expression patterns that support pro-inflammatory signaling, phagocytosis, and metabolic reprogramming. While this is a depiction of microglia transcriptome alterations in response to chronic hyperglycemia in the STZ mouse, we can identify shared patterns with similar studies. High glucose stimulation of microglia in vitro results in upregulation of *Tnf* and *Ccl2* through reactive oxygen species and nuclear factor kappa B pathways (74). Additionally, whole-retina single-cell RNA sequencing studies have reported on microglia-derived production of *Il1b* and metabolic reprogramming that may support inflammation in DR (75). Energetic needs of phagocytic macrophages favor a reduction in glucose uptake and glycolysis while increasing fatty acid oxidation and lipid metabolism, which are consistent with what we report in the present study (16, 76). While these features have been described as a feature of less inflammatory microglia, the combination of metabolic reprogramming and pro-inflammatory priming we observe may underscore a more complex and dynamic role that microglia play in early DR (77). Furthermore, without implementation of single-cell RNA sequencing, we cannot rule out the possibility of heterogeneous microglial subpopulations that may serve divergent roles in pathogenesis.

The leading observation from our RNA-Seq analysis is that CD200R isoforms expressed in retinal microglia are upregulated during early-stage DR. Increased microglial expression of CD200R correlates with their activation and disease pathogenesis (58, 78). CD200 is a transmembrane glycoprotein expressed by neurons and epithelial cells that, upon interacting with its receptor, attenuates immune responses (59). Interestingly, decreased expression of CD200 in CNS neurons, or blocking of CD200R binding, correlates with increases in myeloid cell CD200R expression and neurodegeneration (57, 79, 80). In the retina, this paradigm has also been shown to play roles in animal models of experimental autoimmune uveitis and glaucoma, suggesting that this signaling axis may play a role in other retinal diseases (81, 82). Here, we report that CD200 expression decreases broadly in the inner retinas of STZ-induced diabetic mice. Furthermore, we observe loss of CD200 expression in AC subtypes in diabetic mice, which correlates with contact by activated microglia and inflammation in the retina. In proposing that an imbalance in neuronal CD200 and microglial CD200R contributes in part to microglia-mediated retinopathy, we attempted to enhance microglial CD200R signaling via CD200Fc. Similar to benefits shown in other disease models, we show that CD200Fc attenuates high glucose-induced inflammation, transcriptomic alterations, and phagocytosis in vitro (60, 61, 83). More importantly, we show that CD200Fc therapy at a single time point prevents visual dysfunction, microglial activation, and retinal inflammation in vivo 1 mo later, providing an avenue to treat early-stage DR in the mouse. However, further testing will be necessary to determine whether CD200Fc treatment limits microglial phagocytic capacity in vivo, prevents neurodegeneration of amacrine cells and other key cell types, and sustains therapeutic benefits beyond the short experimental window we investigate in the present study. To this end, future work will need to investigate whether long-term inhibition of microglia via

CD200-CD200R signaling dampens potentially beneficial roles of this cell type and others within the diabetic retinal milieu.

Overall, this study represents a significant advancement in our understanding of inner retinal degeneration during early-stage DR. Microglia dominate the local immune environment of the retina and are actively involved in concurrent neurodegeneration and visual dysfunction. Within this landscape of early disease, we have identified CD200-CD200R dysregulation as a mechanism underlying microglia-mediated retinopathy in the diabetic mouse. Furthermore, we provide strong evidence of the therapeutic value that CD200R signaling provides in the case of hyperglycemia-induced microglia activation. Through this work, we have created a framework for future development of this therapy.

Materials and Methods

We generated mouse models of diabetes with streptozotocin and microglia ablation. We performed flow cytometry, in vivo imaging, electroretinography, immunohistochemistry, TEM, 3D image reconstruction and analysis, RNA sequencing with qPCR validation, and ligand–receptor analysis. We further validated and interrogated these findings with qPCR, immunostaining, and high glucose media challenge of a microglia cell line. We also tested the therapeutic benefit of CD200Fc treatment in vitro and in vivo using intravitreal injections in mice. Experimental details are described in *SI Appendix*.

Data, Materials, and Software Availability. Raw sequencing files and processed data matrices for flow-sorted microglia RNA sequencing data have been deposited in GEO with the following accession number: GSE222005. Similar files for CD200Fc-treated BV2 microglia RNA sequencing data have been deposited in GEO with the following accession number: GSE238008. These sequencing datasets are publicly available as of the date of the publication. All other data are included in the manuscript and/or supporting information (84, 85).

1. S. R. Flaxman *et al.*, Global causes of blindness and distance vision impairment 1990–2020: A systematic review and meta-analysis. *Lancet Global Health* **5**, e1221–e1234 (2017).
2. P. Saeedi *et al.*, Global and regional diabetes prevalence estimates for 2019 and projections for 2030 and 2045: Results from the International Diabetes Federation Diabetes Atlas, 9th edition. *Diabetes Res. Clin. Pract.* **157**, 107843 (2019).
3. W. Wang, A. Lo, Diabetic retinopathy: Pathophysiology and treatments. *IJMS* **19**, 1816 (2018).
4. E. H. Sohn *et al.*, Retinal neurodegeneration may precede microvascular changes characteristic of diabetic retinopathy in diabetes mellitus. *Proc. Natl. Acad. Sci. U.S.A.* **113**, E2655–E2664 (2016).
5. S. F. Abcouwer, T. W. Gardner, Diabetic retinopathy: Loss of neuroretinal adaptation to the diabetic metabolic environment. *Ann. N.Y. Acad. Sci.* **1311**, 174–190 (2014).
6. T. S. Kern, B. A. Berkowitz, Photoreceptors in diabetic retinopathy. *J. Diabetes Invest.* **6**, 371–380 (2015).
7. S. H. Sinclair, S. S. Schwartz, Diabetic retinopathy-an underdiagnosed and undertreated inflammatory, neuro-vascular complication of diabetes. *Front. Endocrinol.* **10**, 843 (2019).
8. A. Cerani *et al.*, Neuron-derived semaphorin 3A is an early inducer of vascular permeability in diabetic retinopathy via neuropilin-1. *Cell Metab.* **18**, 505–518 (2013).

9. A. Honasoge, E. Nudleman, M. Smith, R. Rajagopal, Emerging insights and interventions for diabetic retinopathy. *Curr. Diab Rep.* **19**, 100 (2019).

10. E. J. Duh, J. K. Sun, A. W. Stitt, Diabetic retinopathy: Current understanding, mechanisms, and treatment strategies. *JCI Insight* **2**, e93751 (2017).

11. P. S. Silva, J. K. Sun, L. P. Aiello, Role of steroids in the management of diabetic macular edema and proliferative diabetic retinopathy. *Seminars Ophthalmol.* **24**, 93–99 (2009).

12. M. Bolinger, D. Antonetti, Moving past anti-VEGF: Novel therapies for treating diabetic retinopathy. *IJMS* **17**, 1498 (2016).

13. L. Chen, P. Yang, A. Kijlstra, Distribution, markers, and functions of retinal microglia. *Ocular Immunol. Inflamm.* **10**, 27–39 (2002).

14. X. Wang et al., Requirement for microglia for the maintenance of synaptic function and integrity in the mature retina. *J. Neurosci.* **36**, 2827–2842 (2016).

15. M. Karlstetter, S. Ebert, T. Langmann, Microglia in the healthy and degenerating retina: Insights from novel mouse models. *Immunobiology* **215**, 685–691 (2010).

16. R. C. Paolicelli et al., Microglia states and nomenclature: A field at its crossroads. *Neuron* **110**, 3458–3483 (2022).

17. L. M. De Biase et al., Local cues establish and maintain region-specific phenotypes of basal ganglia microglia. *Neuron* **95**, 341–356.e6 (2017).

18. C. A. Colton, Heterogeneity of microglial activation in the innate immune response in the brain. *J. Neuroimmune Pharmacol.* **4**, 399–418 (2009).

19. H. Keren-Shaul et al., A unique microglia type associated with restricting development of Alzheimer's disease. *Cell* **169**, 1276–1290.e17 (2017).

20. T. R. Hammond et al., Single-cell RNA sequencing of microglia throughout the mouse lifespan and in the injured brain reveals complex cell-state changes. *Immunity* **50**, 253–271.e6 (2019).

21. L. Zhao et al., Microglial phagocytosis of living photoreceptors contributes to inherited retinal degeneration. *EMBO Mol. Med.* **7**, 1179–1197 (2015).

22. H. Zeng et al., Identification of sequential events and factors associated with microglial activation, migration, and cytotoxicity in retinal degeneration in *rd* mice. *Invest. Ophthalmol. Vis. Sci.* **46**, 2992 (2005).

23. E. G. O'Koren et al., Microglial function is distinct in different anatomical locations during retinal homeostasis and degeneration. *Immunity* **50**, 723–737.e7 (2019).

24. X.-X. Zeng, Y.-K. Ng, E.-A. Ling, Neuronal and microglial response in the retina of streptozotocin-induced diabetic rats. *Vis. Neurosci.* **17**, 463–471 (2000).

25. H. Zeng, Microglial activation in human diabetic retinopathy. *Arch Ophthalmol.* **126**, 227 (2008).

26. Y. Xia et al., Retinal astrocytes and microglia activation in diabetic retinopathy rhesus monkey models. *Curr. Eye Res.* **47**, 297–303 (2022).

27. J. G. Grigsby et al., The role of microglia in diabetic retinopathy. *J. Ophthalmol.* **2014**, 1–15 (2014).

28. K. A. Church et al., Microglia depletion elicits neuroprotective effects to alleviate vascular damage and neuronal cell loss in the diabetic retina. *J. Immunol.* **208**, 54.14-54.14 (2022).

29. H. Xu, M. Chen, Diabetic retinopathy and dysregulated innate immunity. *Vision Res.* **139**, 39–46 (2017).

30. A. Rübsam, S. Parikh, P. Fort, Role of inflammation in diabetic retinopathy. *IJMS* **19**, 942 (2018).

31. F. S. Sorrentino, M. Allkabes, G. Salsini, C. Bonifazzi, P. Perri, The importance of glial cells in the homeostasis of the retinal microenvironment and their pivotal role in the course of diabetic retinopathy. *Life Sci.* **162**, 54–59 (2016).

32. E. Rungger-Brändle, A. A. Dosso, P. M. Leuenberger, Glial reactivity, an early feature of diabetic retinopathy. *Invest. Ophthalmol. Vis. Sci.* **41**, 1971–1980 (2000).

33. H. Zong et al., Hyperglycaemia-induced pro-inflammatory responses by retinal Müller glia are regulated by the receptor for advanced glycation end-products (RAGE). *Diabetologia* **53**, 2656–2666 (2010).

34. F. Su, H. Yi, L. Xu, Z. Zhang, Fluoxetine and S-citalopram inhibit M1 activation and promote M2 activation of microglia in vitro. *Neuroscience* **294**, 60–68 (2015).

35. D. Lam, S. Lively, L. C. Schlichter, Responses of rat and mouse primary microglia to pro- and anti-inflammatory stimuli: Molecular profiles, K+ channels and migration. *J. Neuroinflamm.* **14**, 166 (2017).

36. T. A. Siddiqui, S. Lively, L. C. Schlichter, Complex molecular and functional outcomes of single versus sequential cytokine stimulation of rat microglia. *J. Neuroinflamm.* **13**, 66 (2016).

37. R. M. Brucklacher et al., Whole genome assessment of the retinal response to diabetes reveals a progressive neurovascular inflammatory response. *BMC Med Genomics* **1**, 26 (2008).

38. B. L. Furman, Streptozotocin-induced diabetic models in mice and rats. *Curr. Protoc.* **1**, 5.47.1–5.47.20 (2021).

39. J. Sergeys et al., Longitudinal in vivo characterization of the streptozotocin-induced diabetic mouse model: Focus on early inner retinal responses. *Invest. Ophthalmol. Vis. Sci.* **60**, 807 (2019).

40. H. W. Van Dijk et al., Selective loss of inner retinal layer thickness in Type 1 diabetic patients with minimal diabetic retinopathy. *Invest. Ophthalmol. Vis. Sci.* **50**, 3404 (2009).

41. J. Peng, Q. Zou, M.-J. Chen, C.-L. Ma, B.-M. Li, Motor deficits seen in microglial ablation mice could be due to non-specific damage from high dose diphtheria toxin treatment. *Nat. Commun.* **13**, 3874 (2022).

42. F. Lei et al., CSF1R inhibition by a small-molecule inhibitor is not microglia specific; affecting hematopoiesis and the function of macrophages. *Proc. Natl. Acad. Sci. U.S.A.* **117**, 23336–23338 (2020).

43. J. Bruttger et al., Genetic cell ablation reveals clusters of local self-renewing microglia in the mammalian central nervous system. *Immunity* **43**, 92–106 (2015).

44. M. T. Pardue et al., Rodent hyperglycemia-induced inner retinal deficits are mirrored in human diabetes. *Trans. Vis. Sci. Tech.* **3**, 6 (2014).

45. L. Wachtmeister, Oscillatory potentials in the retina: What do they reveal? *Prog. Retinal Eye Res.* **17**, 485–521 (1998).

46. J. Dai et al., Contribution of GABAa, GABAc and glycine receptors to rat dark-adapted oscillatory potentials in the time and frequency domain. *Oncotarget* **8**, 77696–77709 (2017).

47. M. J. Gastinger, R. S. J. Singh, A. J. Barber, Loss of cholinergic and dopaminergic amacrine cells in streptozotocin-diabetic rat and ins2 ^{Akita}-diabetic mouse retinas. *Invest. Ophthalmol. Vis. Sci.* **47**, 3143 (2006).

48. S.-H. Park et al., Apoptotic death of photoreceptors in the streptozotocin-induced diabetic rat retina. *Diabetologia* **46**, 1260–1268 (2003).

49. Y. Okunuki et al., Microglia inhibit photoreceptor cell death and regulate immune cell infiltration in response to retinal detachment. *Proc. Natl. Acad. Sci. U.S.A.* **115**, E6264–E6273 (2018).

50. K. Bisht et al., Dark microglia: A new phenotype predominantly associated with pathological states. *Glia* **64**, 826–839 (2016).

51. J. R. Anderson et al., Exploring the retinal connectome. *Mol. Vis* **17**, 355–379 (2011).

52. C. Sousa et al., Single-cell transcriptomics reveals distinct inflammation-induced microglia signatures. *EMBO Rep.* **19**, e46171 (2018).

53. I. M. Chiu et al., A neurodegeneration-specific gene-expression signature of acutely isolated microglia from an amyotrophic lateral sclerosis mouse model. *Cell Rep.* **4**, 385–401 (2013).

54. S. A. Mills et al., Fractalkine-induced microglial vasoregulation occurs within the retina and is altered early in diabetic retinopathy. *Proc. Natl. Acad. Sci. U.S.A.* **118**, e2112561118 (2021).

55. F. Guillaumond et al., Krüppel-like factor KLF10 is a link between the circadian clock and metabolism in liver. *Mol. Cell. Biol.* **30**, 3059–3070 (2010).

56. S. Cabello-Aguilar et al., SingleCellSignalR: Inference of intercellular networks from single-cell transcriptomics. *Nucleic Acids Res.* **48**, e55–e55 (2020).

57. M. Oria et al., CD200-CD200R imbalance correlates with microglia and pro-inflammatory activation in rat spinal cords exposed to amniotic fluid in retinoic acid-induced spina bifida. *Sci. Rep.* **8**, 10638 (2018).

58. S. Zhao et al., CD200-CD200R1 signaling pathway regulates neuroinflammation after stroke. *Brain Behav.* **10**, e01882 (2020).

59. K. Kotwica-Mojzych, B. Jodłowska-Jędrych, M. Mojzych, CD200:CD200R interactions and their importance in immunoregulation. *IJMS* **22**, 1602 (2021).

60. L. Jiang et al., CD200Fc reduces TLR4-mediated inflammatory responses in LPS-induced rat primary microglial cells via inhibition of the NF-κB pathway. *Inflamm. Res.* **65**, 521–532 (2016).

61. M. Hernangómez et al., CD200R1 agonist attenuates glial activation, inflammatory reactions, and hypersensitivity immediately after its intrathecal application in a rat neuropathic pain model. *J. Neuroinflamm.* **13**, 43 (2016).

62. J. Iannucci, H. V. Rao, P. Grammas, High glucose and hypoxia-mediated damage to human brain microvessel endothelial cells induces an altered, pro-inflammatory phenotype in BV-2 microglia in vitro. *Cell Mol. Neurobiol.* **42**, 985–996 (2022).

63. J. Shi, L. Hua, D. Harmer, P. Li, G. Ren, "Cre driver mice targeting macrophages" in *Methods in Molecular Biology*, G. Rousselet, Ed. (Springer, New York, 2018), pp. 263–275.

64. E. Beli et al., CX3CR1 deficiency accelerates the development of retinopathy in a rodent model of type 1 diabetes. *J. Mol. Med.* **94**, 1255–1265 (2016).

65. H. Yokomizo et al., Retinol binding protein 3 is increased in the retina of patients with diabetes resistant to diabetic retinopathy. *Sci. Transl. Med.* **11**, eaau6627 (2019).

66. K. Miyamoto et al., Prevention of leukostasis and vascular leakage in streptozotocin-induced diabetic retinopathy via intercellular adhesion molecule-1 inhibition. *Proc. Natl. Acad. Sci. U.S.A.* **96**, 10836–10841 (1999).

67. A. M. Olivares et al., Animal models of diabetic retinopathy. *Curr. Diab. Rep.* **17**, 93 (2017).

68. A. A. Like, A. A. Rossini, Streptozotocin-induced pancreatic insulitis: New model of diabetes mellitus. *Science* **193**, 415–417 (1976).

69. P. M. Martin, P. Roon, T. K. Van Ells, V. Ganapathy, S. B. Smith, Death of retinal neurons in streptozotocin-induced diabetic mice. *Invest. Ophthalmol. Vis. Sci.* **45**, 3330 (2004).

70. A. Ferro, Y. S. S. Auguste, L. Cheadle, Microglia, cytokines, and neural activity: Unexpected interactions in brain development and function. *Front. Immunol.* **12**, 703527 (2021).

71. M. Hayden, D. Grant, A. Aroor, V. DeMarco, Ultrastructural remodeling of the neurovascular unit in the female diabetic db/db model-part II: Microglia and mitochondria. *Neuroglia* **1**, 311–326 (2018).

72. H. El Hajj et al., Ultrastructural evidence of microglial heterogeneity in Alzheimer's disease amyloid pathology. *J. Neuroinflamm.* **16**, 87 (2019).

73. C.-F. Hsieh, C.-K. Liu, C.-T. Lee, L.-E. Yu, J.-Y. Wang, Acute glucose fluctuation impacts microglial activity, leading to inflammatory activation or self-degradation. *Sci. Rep.* **9**, 840 (2019).

74. Y. Quan, C. Jiang, B. Xue, S. Zhu, X. Wang, High glucose stimulates TNFα and MCP-1 expression in rat microglia via ROS and NF-κB pathways. *Acta Pharmacol. Sin* **32**, 188–193 (2011).

75. K. Lv et al., Integrated multi-omics reveals the activated retinal microglia with intracellular metabolic reprogramming contributes to inflammation in STZ-induced early diabetic retinopathy. *Front. Immunol.* **13**, 942768 (2022).

76. O. Kolliniati, E. Ieronymaki, E. Vergadi, C. Tsatsanis, Metabolic regulation of macrophage activation. *J. Innate Immun.* **14**, 51–68 (2022).

77. K. Mehla, P. K. Singh, Metabolic regulation of macrophage polarization in cancer. *Trends Cancer* **5**, 822–834 (2019).

78. K. Lunnon et al., Systemic inflammation modulates Fc receptor expression on microglia during chronic neurodegeneration. *J. Immunol.* **186**, 7215–7224 (2011).

79. S. Zhang et al., CD200-CD200R dysfunction exacerbates microglial activation and dopaminergic neurodegeneration in a rat model of Parkinson's disease. *J. Neuroinflamm.* **8**, 154 (2011).

80. A. Lyons et al., CD200 ligand-receptor interaction modulates microglial activation in vivo and in vitro: A role for IL-4. *J. Neurosci.* **27**, 8309–8313 (2007).

81. C. Broderick et al., Constitutive retinal CD200 expression regulates resident microglia and activation state of inflammatory cells during experimental autoimmune uveoretinitis. *Am. J. Pathol.* **161**, 1669–1677 (2002).

82. S. Taylor et al., Involvement of the CD200 receptor complex in microglia activation in experimental glaucoma. *Exp. Eye Res.* **92**, 338–343 (2011).

83. Y. Liu et al., CD200R1 agonist attenuates mechanisms of chronic disease in a murine model of multiple sclerosis. *J. Neurosci.* **30**, 2025–2038 (2010).

84. C. W. Pfeifer, R. S. Apte, RNA-seq of STZ-treated mouse retinal microglia cells. Gene Expression Omnibus. https://www.ncbi.nlm.nih.gov/geo/query/acc.cgi?acc=GSE222005. Deposited 2 January 2023.

85. C. W. Pfeifer, R. S. Apte, RNA-seq of BV2 cultured microglia following high glucose and CD200Fc treatments. Gene Expression Omnibus. https://www.ncbi.nlm.nih.gov/geo/query/acc.cgi?acc=GSE238008. Deposited 21 July 2023.